Letter

Magnetic structure of Ce_3TiBi_5 and its relation to current-induced magnetization

Nicolas Gauthier [1,*] Romain Sibille,[2] Vladimir Pomjakushin,[2] Øystein S. Fjellvåg [2,3] James Fraser [4]
Mathieu Desmarais [4] Andrea D. Bianchi [4,5] and Jeffrey A. Quilliam[1]

[1]*Institut Quantique, Département de physique & Regroupement Québécois sur les Matériaux de Pointe (RQMP),*
Université de Sherbrooke, Sherbrooke, Québec J1K 2R1, Canada
[2]*Laboratory for Neutron Scattering and Imaging, Paul Scherrer Institute, CH-5232 Villigen, Switzerland*
[3]*Department for Hydrogen Technology, Institute for Energy Technology, PO Box 40, NO-2027 Kjeller, Norway*
[4]*Département de Physique & Regroupement Québécois sur les Matériaux de Pointe (RQMP),*
Université de Montréal, Montréal, Québec H2V 0B3, Canada
[5]*Institut Courtois, Université de Montréal, Montréal, Québec H2V 0B3, Canada*

The control of magnetization using electric fields has been extensively studied in magnetoelectric multiferroic insulating materials while changes in magnetization in bulk metals caused by electric currents have attracted less attention. The recently discovered metallic magnet Ce_3TiBi_5 has been reported to exhibit current-induced magnetization. Here we determined the magnetic structure of Ce_3TiBi_5 using neutron diffraction, aiming to understand the microscopic origin of this magnetoelectric phenomenon in a metal. We established that the antiferromagnetic order emerging below $T_N = 5$ K is a cycloid order described by $P6_3/mcm.1'(0, 0, g)00sss$ with small moment sizes of 0.50(2) μ_B and propagation vector $\mathbf{k} = (0, 0, 0.386)$. Surprisingly, the symmetry of this magnetic structure is inconsistent with the presence of current-induced magnetization and potential origins of this inconsistency with previous results are discussed. Additionally, our results suggest that moments order along their hard magnetic direction in Ce_3TiBi_5, a phenomenon which has been observed in other Kondo systems.

DOI: 10.1103/PhysRevB.109.L140405

Introduction. The possibility to induce magnetization with an electric field, or an electric polarization with a magnetic field is a well known effect in magnetoelectric multiferroic materials and of relevance to novel electronic devices [1]. These magnetoelectric effects can arise due to so-called toroidal orders. Toroidal orders are described by combined electric and magnetic orders and exist in various multiferroic insulators [2,3]. In contrast, few examples of toroidal orders in metals have been found. Interestingly, theoretical work has shown that, in metals without local inversion symmetry, toroidal order modifies the electronic band structure and leads to anisotropic Hall responses as well as current-induced magnetization [4]. Experimentally, magnetization induced by an electric current in a metallic magnet has only been recently demonstrated for UNi_4B [5]. The reported vortexlike magnetic structure of UNi_4B generates a toroidal moment and has been considered to be a fundamental element in the theoretical description of this effect [4]. However, magnetoelectric responses not expected by this theory were also observed and an alternative theory suggesting a more complex magnetic structure exists [6].

The Ce_3TiBi_5 compound is another interesting candidate to study magnetoelectric effects caused by toroidal order in a metal without local inversion symmetry. This material, first synthesized only recently [7], crystallizes in a hexagonal structure (space group $P6_3/mcm$) with Ce zigzag chains along the c axis, as shown in Fig. 1(b). It exhibits an antiferromagnetic order below $T_N = 5.0$ K, as evidenced by resistivity,

magnetic susceptibility, and specific heat measurements [7]. Its large Sommerfeld coefficient of $\gamma = 210$ mJ/(K^2 Ce-mol) indicates heavy fermion behavior. Its magnetic susceptibility exhibits a peculiar anisotropic temperature dependence [7,8]. The susceptibility in the ab plane is more than three times the c-axis susceptibility below 20 K, suggesting a preferred moment orientation in the ab plane. Yet, the in-plane susceptibility does not reduce below T_N as in a typical antiferromagnet but continues to increase with decreasing temperature. Instead, typical antiferromagnetic behavior is observed for the significantly smaller c-axis susceptibility, suggesting an ordering along the magnetic hard axis [9].

Interestingly, it was observed that applying a current along the a axis in the presence of the antiferromagnetic order induces a magnetization along the c axis in Ce_3TiBi_5 [10]. Although numerous isostructural analogs of Ce_3TiBi_5 are being investigated [11–17], only Ce_3TiBi_5 has been reported to host current-induced magnetization up to now. To explain the magnetoelectric effect in Ce_3TiBi_5, a theoretical work suggested a potential magnetic structure, associated with a ferrotoroidal order [18]. Nevertheless, its experimental determination is required to obtain a convincing understanding of this phenomenon. In this Letter, we report neutron diffraction measurements of Ce_3TiBi_5 and determine its magnetic structure, establishing that it is different from the theoretical proposal. Our results resolve ambiguities associated with its magnetic susceptibility but raise doubts about the intrinsic nature of the observed current-induced magnetization.

Methods. Single crystals of Ce_3TiBi_5 were grown using the Bi self-flux method [7]. Starting material of cerium (99.9%), titanium (99.99%), and bismuth (99.999%) in a ratio 3:1:20

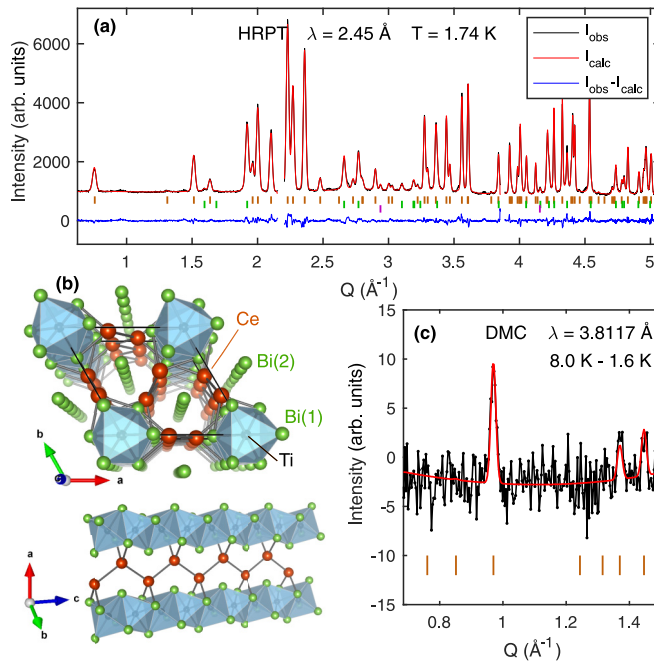*Corresponding author: nicolas.gauthier@inrs.ca

FIG. 1. (a) Powder neutron diffraction pattern of Ce_3TiBi_5 measured with the HRPT diffractometer. Dark orange and green ticks indicate peak positions of the Ce_3TiBi_5 phase and a Bi impurity phase, respectively. Purple ticks indicate vanadium peaks from the sample container. Regions at $\sim$2.2 Å^{-1} and $\sim$3.9 Å^{-1} are associated with dominant peaks of $CeTi_3Bi_4$ impurities and were excluded. (b) Crystallographic structure of Ce_3TiBi_5, showing the Ce zigzag chains along the c axis. (c) Difference powder pattern between 8.0 K and 1.6 K measured with the DMC diffractometer. Three magnetic peaks are observed and are well described by the $P6_3/mcm.1'(0, 0, g)00sss$ magnetic structure.

TABLE I. Crystallographic parameters obtained from refinement of HRPT diffraction patterns. Atomic positions are Ce at $6g$ (x, 0, 1/4), Ti at $2b$ (0, 0, 0), Bi(1) at $6g$ (x, 0, 1/4), and Bi(2) at $4d$ (1/3, 2/3, 0). Data obtained 1.74 K have 3.5 times more statistics than the 8 K data, justifying the difference in χ^2 between datasets.

T (K)	1.74	8.0
a (Å)	9.58146(4)	9.58140(5)
c (Å)	6.40091(4)	6.40106(4)
Vol. (Å^3)	508.904(4)	508.909(4)
x_{Ce}	0.6179(2)	0.6177(2)
$x_{Bi(1)}$	0.25613(9)	0.2562(1)
R_{wp}	7.11	8.29
R_{exp}	2.91	5.47
χ^2	5.96	2.30
R_{Bragg}	2.33	2.20

were placed in an alumina crucible. Growth batch A was obtained by sealing the crucible in a quartz ampoule with argon. The ampoule was heated to 1000 °C at 50 °C/h, kept at this temperature for 11 h and cooled down to 500 °C at a rate of 2 °C/h. The excess Bi was removed by centrifugation immediately after removing the ampoule from the oven. The obtained needle-shaped crystals are air sensitive: in air they decompose in a few days and burn when broken or crushed. They were kept and handled in a controlled atmosphere in a glove box, and transported to experiments in sealed containers. The Ce_3TiBi_5 phase was confirmed by x-ray powder diffraction using a domed sample holder with crystals powderized in the glove box. Several large $\sim$50 mg single crystals were obtained in this batch and one with dimensions $\sim$5×1×1 mm^3 was used for the single-crystal neutron diffraction experiment. Growth batch B was obtained by sealing the alumina crucible in a quartz ampoule under vacuum. In that case, the ampoule was kept at 1000 °C for 15 h and cooled down at a rate of 1 °C/h, with all the other conditions identical to batch A. The resulting crystals were slightly smaller than in batch A. Needle-shaped crystals were isolated and powderized in a glove box. The obtained 3.4 g powder was used for the powder neutron diffraction experiments.

Powder neutron diffraction measurements were performed using the HRPT and DMC instruments at SINQ, Paul Scher-rer Institut. The 3.4 g powder was loaded in a vanadium can and sealed in a helium atmosphere. The sample was loaded in an orange cryostat and data were collected using neutron wavelengths $\lambda = 2.45$ Å and 3.81 Å for HRPT and DMC instruments, respectively. Single-crystal diffraction measurements were performed on the ZEBRA diffractometer at SINQ. The 50 mg sample was mounted in a Joule-Thomson cryostat in a four-circle geometry and measured with $\lambda = 1.383$ Å neutrons. Data were analyzed with the FULLPROF program [19] and figures of crystallographic and magnetic structures were generated using the VESTA software [20].

Experimental results. High-resolution powder neutron diffraction patterns were measured using the HRPT diffractometer at $T = 1.74$ K and 8 K, i.e., below and above T_N. The pattern and associated refinement for $T = 1.74$ K is presented in Fig. 1(a). The pattern is dominated by the Ce_3TiBi_5 phase but a large weight fraction of Bi impurity phase ($\sim$18%) is present, likely originating from excess Bi flux. The refinement of the Ce_3TiBi_5 confirms the previously established $P6_3/mcm$ structure [7], illustrated in Fig. 1(b). The refined crystallographic parameters for both temperatures are reported in Table I. There is no evidence for any structural distortion. Except for a small contraction along the c axis, all refined parameters are temperature independent within the measurement uncertainties. No new peaks associated with magnetic order were observed for $T < T_N$ in this measurement due to weak magnetic scattering at short neutron wavelength.

Magnetic peaks were revealed by measurements on the DMC diffractometer, optimized for magnetic structure determination. A difference pattern of 1.6 K and 8 K data, presented in Fig. 1(c), exhibits a clear peak at $Q = 0.97$ Å^{-1} as well as two weaker peaks around 1.4 Å^{-1}. These peaks are insufficient to establish unambiguously the propagation vector associated with the antiferromagnetic order. The propagation vector $\mathbf{k} = (0, 0, \delta)$ with $\delta = 0.386$ was determined by single-crystal diffraction with the ZEBRA diffractometer. Figure 2(a) shows the temperature dependence of the magnetic Bragg peak $\mathbf{Q} = (-1, 1, -0.614)$. The peak position is unaffected by temperature, indicating that the incommensurate parameter δ is temperature independent. The peak intensity decreases when increasing temperature from 1.6 K to 4 K and is absent at $T = 6$ K $> T_N$. The intensity at the top of the magnetic
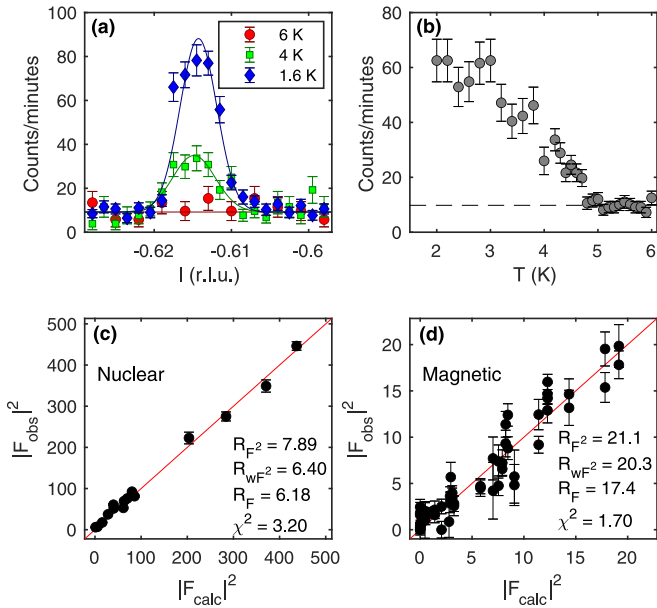
FIG. 2. (a) Temperature dependence of the magnetic Bragg peak $\mathbf{Q} = (-1, 1, l)$, showing that the incommensurate value does not change with temperature. Data were fitted with a Gaussian function. (b) Temperature dependence of the scattering intensity at the Bragg peak position $\mathbf{Q} = (-1, 1, -0.614)$ showing the emergence of the magnetic order parameter at $T_N = 5$ K. (c) Result of the nuclear structure refinement at $T = 1.6$ K, represented by the comparison of $|F_{obs}|^2$ and $|F_{calc}|^2$, the observed and calculated squared structure factors, respectively. (d) Result of the $P6_3/mcm.1'(0, 0, g)00sss$ magnetic structure refinement in the same conditions.

Bragg peak decreases with increasing temperature and reaches the background intensity at T_N [Fig. 2(b)], confirming that it arises from the magnetic order.

Nuclear and magnetic Bragg peaks were collected at $T = 1.6$ K to perform crystallographic and magnetic structure refinements using the FULLPROF program [19]. The scaling factor obtained from the nuclear data set refinement, shown in Fig. 2(c), was used to determine absolute moment sizes. Magnetic peaks were collected for both $+\mathbf{k}$ and $-\mathbf{k}$ and refined jointly. Possible magnetic structures were determined from a symmetry analysis using the ISODISTORT tool [21,22]. The propagation vector $\mathbf{k}$ corresponds to the Δ point of the Brillouin zone and leads to six potential magnetic irreducible representations labeled $m\Delta_i$ with $i = 1$–6. Considering the incommensurate nature of $\mathbf{k}$, we describe the magnetic structure using the magnetic superspace group (MSG) formalism [23]. Superspace groups go beyond the usual three-dimensional space groups by assuming one or more additional dimensions to treat incommensurate structures. Magnetic space groups consider the time-reversal symmetry operator to account for magnetism. MSGs combine both concepts. The DMC difference pattern is well accounted for by considering MSGs generated by either $m\Delta_2$ or $m\Delta_5$. The acceptable $m\Delta_5$ MSGs all contain the $m\Delta_2$ distortion modes but have a lower symmetry than the $m\Delta_2$ MSGs. Therefore, the $m\Delta_5$ MSGs are ignored to keep only the highest symmetry solutions generated by $m\Delta_2$. The candidate MSGs are $P6_3/mcm.1'(0, 0, g)00sss$ and $P6_3cm.1'(0, 0, g)0sss$, with the
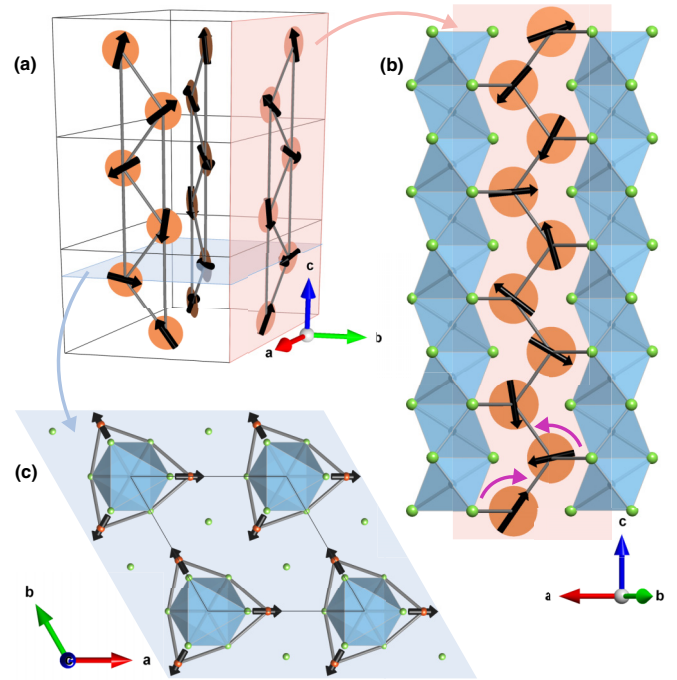

FIG. 3. (a) Magnetic structure of Ce₃TiBi₅. For each zigzag chain, the moments are confined in a plane, represented by the orange circle at each Ce site. The ac plane indicated in red and the ab plane indicated in blue are presented in (b) and (c), respectively. The ordering on the zigzag chain is explicitly presented in (b). The two sides of the zigzag chain form a cycloid order but with opposite rotation directions. The moments on left side of the zigzag chain rotate clockwise from one site to the next along the c axis, as illustrated by the purple arrow. In contrast, the moments on the right side rotate counterclockwise. The ab plane presented in (c) illustrates the ordering of the in-plane magnetic components between the chains.

main difference being the loss of inversion symmetry in the latter.

Refinement of the ZEBRA magnetic data sets also indicates that the two $m\Delta_2$-generated MSGs are the best solutions with agreement factors $R_F = 17.4$ and 21.0 for $P6_3/mcm.1'(0, 0, g)00sss$ and $P6_3cm.1'(0, 0, g)0sss$, respectively. Comparable agreement factors can only be obtained with $m\Delta_5$-generated MSGs, which are disregarded in the following due to their lower symmetry. Considering that both $m\Delta_2$ solutions provide comparable agreement with the data, the first, higher symmetry $P6_3/mcm.1'(0, 0, g)00sss$ structure is assumed to be the correct description of Ce₃TiBi₅ antiferromagnetic order. The refinement result for this MSG is shown in Fig. 2(d) and the obtained magnetic structure is presented in Fig. 3. It corresponds to a cycloid order propagating along the c axis. For each zigzag chain, the moments lie in the plane containing that zigzag chain. The incommensurate value δ leads to a moment rotation of 139° per unit cell along the c axis. It is noteworthy that the moments on the two legs of the zigzag chain rotate in opposite directions, and models with moments rotating in the same direction cannot describe our data satisfactorily. For the zigzag chain illustrated in Fig. 3(b), the left side of the chain rotates clockwise and the right side of the chain rotates counterclockwise, as indicated by the purple

arrows. The relative phase between these opposite rotations is symmetry enforced. This leads to moment components along the c axis that are predominantly aligned ferromagnetically for nearest-neighbor bonds, while the transverse moment components approach an antiferromagnetic alignment. Such alignment suggests that anisotropic interactions are responsible for the opposite rotations and their relative phase. We note that counterrotating cycloids were also reported in iridates with anisotropic Kitaev interactions [24].

The evolution of the magnetic moments $\mathbf{M}_i$ along the propagation axis can be expressed by

$$\mathbf{M}_i = \mathbf{M}_i^{\sin} \sin(2\pi\delta Z_i) + \mathbf{M}_i^{\cos} \cos(2\pi\delta Z_i), \qquad (1)$$

where Z_i is the position along c of site i in lattice units. Moments $\mathbf{M}_i$ within one unit cell are related to each other by the symmetry operators of the MSGs. For the $P6_3/mcm.1'(0,0,g)00sss$ group, $\mathbf{M}_i^{\cos}$ and $\mathbf{M}_i^{\sin}$ are constrained to be orthogonal and lie in the xz plane. Here, x is along the local twofold axis while z is along the c axis. Specifically, the magnetic components are given by $\mathbf{M}_i^{\sin} = (M_x^{\sin}, 0, 0)$ and $\mathbf{M}_i^{\cos} = (0, 0, M_z^{\cos})$. This describes a conventional cycloid order when $M_x^{\sin}$ and $M_z^{\cos}$ are accidentally equal. If $M_x^{\sin} \neq M_z^{\cos}$, it corresponds to a cycloid order with an ellipsoidal envelope having principal axes along x and z. Our single-crystal data refinement presented in Fig. 2(d) suggests a conventional cycloid order with $M_x^{\sin} = -0.50(2)$ μ_B and $M_z^{\cos} = -0.50(2)$ μ_B. The refinement of the DMC difference pattern with the same MSG [red line on Fig. 1(c)] indicates slightly smaller moment sizes of $M_x^{\sin} = -0.40(2)$ μ_B and $M_z^{\cos} = 0.37(3)$ μ_B with an incommensurate value $\delta = 0.389(2)$. The goodness of fit and R factors for this refinement are $R_{\rm wp} = 75.0$, $R_{\rm exp} = 78.9$, $\chi^2 = 0.91$, $R_{\rm Bragg} = 21.4$.

For the lower symmetry $P6_3cm.1'(0,0,g)0sss$ group, which breaks inversion symmetry, $\mathbf{M}_i^{\cos}$ and $\mathbf{M}_i^{\sin}$ are still constrained to lie in the xz plane but the orthogonality restriction is removed. Specifically, the magnetic components are given by $\mathbf{M}_i^{\sin} = (M_x^{\sin}, 0, M_z^{\sin})$ and $\mathbf{M}_i^{\cos} = (M_x^{\cos}, 0, M_z^{\cos})$. The added degree of freedom of this MSG compared to $P6_3/mcm.1'(0,0,g)00sss$ allows the generation of a cycloid order with an ellipsoidal envelope with principal axes away from x and z, or of a noncycloid amplitude-modulated order. For this MSG, the single-crystal data refinement leads to magnetic components describing a structure that approximates the cycloid order obtained for the higher symmetry $P6_3/mcm.1'(0,0,g)00sss$ group. χ^2 values were evaluated for various angles θ between $\mathbf{M}_i^{\sin}$ and $\mathbf{M}_i^{\cos}$ while constraining equal amplitudes $|\mathbf{M}_i^{\sin}| = |\mathbf{M}_i^{\cos}|$. For $\theta = 90°$, the structure is identical to the higher symmetry $P6_3/mcm.1'(0,0,g)00sss$ solution. We find that χ^2 values are almost unchanged for $60° < \theta < 120°$ and increase farther away from orthogonality. Therefore, a small distortion of the magnetic structure breaking inversion symmetry would not be in disagreement with our results. We emphasize that the dominant character of the structure remains a cycloid order with moments lying in the plane of the zigzag chain. The same dominant cycloid character is obtained for all the lower-symmetry $m\Delta_5$-generated MSGs that provided comparable agreement factors to the $m\Delta_2$ solutions.

Discussion. Surprisingly, the observation of a single-**k** incommensurate magnetic order in Ce_3TiBi_5 indicates directly that the current-induced magnetization effect is not allowed by symmetry, in clear contradiction with reported experimental results [10]. The presence of a ferrotoroidal order is requisite to the current-induced magnetization effect according to the theoretical model [18], and such orders are only allowed when both inversion and time-reversal symmetries are broken by the magnetic point group. However, the magnetic point group of single-**k** incommensurate phases always includes time-reversal symmetry and consequently cannot have a ferrotoroidal order [23]. In other words, ferrotoroidal order is forbidden in Ce_3TiBi_5 simply by the observation of a single incommensurate propagation vector, regardless of the presence of inversion symmetry, the details of the magnetic structure and its exact MSG. It is therefore hard to reconcile the reported magnetoelectric effect [10] with the observed single-**k** incommensurate magnetic structure. There is no evidence for sample or growth-batch-dependent properties, either in previous results or in our neutron scattering results, that could explain this inconsistency. Specifically in this work, the results from powder and single-crystal measurements performed on two different growth batches are in good agreement.

Ferrotoroidal order would be allowed if an undetected second **k** vector exists and forms a multi-**k** magnetic structure breaking both inversion and time-reversal symmetry. However, we found no evidence for a second **k** vector. All peaks in the powder diffraction pattern are accounted for. Furthermore, using single-crystal diffraction we measured all points within the irreducible Brillouin zone at $Q = 0.97$ Å^{-1}, where the strongest magnetic scattering is observed in the powder pattern, and magnetic scattering was only observed for $\mathbf{k} = (0, 0, \delta)$. Based on this and the good agreement between the magnetic structures determined for powder and single-crystal samples, we can exclude any significant contribution from an additional **k** vector at this Q value. Yet, we cannot generally exclude the existence of an additional **k** vector with weak scattering intensity at any Q value.

While a second, unobservably weak **k** vector cannot be entirely ruled out, our results bring into question the intrinsic nature of the current-induced magnetization effect observed in the challenging experiment reported in Ref. [10]. In the analysis of this work, the temperature-independent part of the current-induced magnetization was attributed to an extrinsic effect, while the temperature-dependent part was associated with the sample's response. However, the extrinsic induced fields depend, in part, on the path of the current inside the sample. With an imperfect contact geometry, this path is affected by the anisotropy of the resistivity and could be modified with temperature if the anisotropy is temperature dependent. In Ce_3TiBi_5, the resistivity anisotropy ratio is $\rho_c/\rho_{ab} \approx 0.2$ between 5 and 10 K while it suddenly drops below T_N, reaching $\rho_c/\rho_{ab} \approx 0.1$ at 2 K [7]. In brief, significant changes of the resistivity anisotropy occur simultaneously with the magnetic order and might generate temperature-dependent extrinsic fields that could be erroneously interpreted as an intrinsic property of the material. Current-induced measurements on samples with different shapes ought to be carried out to investigate this possibility.

While our results indicate that Ce$_3$TiBi$_5$ does not exhibit a ferrotoroidal order and that the current-induced magnetization could be an experimental artifact, its magnetic properties appear unconventional. Interestingly, the established magnetic structure of Ce$_3$TiBi$_5$, together with its peculiar magnetic susceptibility, suggests that Ce$_3$TiBi$_5$ might be another example of an antiferromagnetic Kondo system ordering along the magnetic hard direction [25]. Generally speaking, ordering of moments is expected along the easy axis for isotropic interactions, as the energy gain is proportional to the square of the moment size. However, it was shown theoretically that particle-hole fluctuations in metallic ferromagnets can generate magnetic orders with moments along their hard axes, analogous to the stabilization of an inverted pendulum with vibrations [26]. This counterintuitive phenomenon is in fact common in Kondo ferromagnets, while only a few Kondo antiferromagnets have been shown to fall into this category [9,25]. In Ce$_3$TiBi$_5$, the peculiar magnetic susceptibility can be qualitatively explained by assuming that for each zigzag chain the local hard plane corresponds to the plane of the zigzag chain, and the local easy axis is perpendicular to it. The c-axis susceptibility, probing one component of the hard plane, is weak and clearly exhibits a drop at the antiferromagnetic transition as this component orders. The in-plane susceptibility probes simultaneously the other hard-plane component and the easy-axis one, but is dominated by the easy-axis component, which has a larger susceptibility. As this easy-axis component does not order, the susceptibility continues to grow below T_N while the kink is caused by the weaker hard-plane component.

Another indication of hard-direction ordering is given by the magnetization resulting from fields applied in the ab plane. Indeed, the magnetization starts to saturate at $\sim$1 μ_B/Ce above $H = 7$ T [8], a value that is twice the fully ordered moment in zero field determined here. The polarization of the moments along the easy axis by the field provides a simple explanation for this large magnetization. It cannot be explained by field-induced mixing of higher energy CEF levels, as they are separated by tens of K from the ground-state doublet based on specific heat measurements [8]. In contrast to Ce$_3$TiBi$_5$, the Sb analog Ce$_3$TiSb$_5$ exhibits a more conventional magnetic susceptibility, with its antiferromagnetic transition observed in the largest susceptibility component [13]. Powder neutron diffraction measurements performed on Ce$_3$TiSb$_5$ at $T = 1.5$ K in the antiferromagnetic phase revealed large moment sizes of $\sim$2μ_B and a dominant moment direction transverse to the plane of the zigzag chain [14]. This suggests that Ce$_3$TiSb$_5$ and Ce$_3$TiBi$_5$ have comparable anisotropies but that Ce$_3$TiSb$_5$ orders along the easy axis while Kondo fluctuations drive an ordering in the hard plane for Ce$_3$TiBi$_5$.

In summary, we established the magnetic structure of Ce$_3$TiBi$_5$ to be a cycloid order with moments lying in the plane of the zigzag chain. This structure does not allow a ferrotoroidal order and calls into question the intrinsic nature of the reported current-induced magnetization effect. The determined magnetic structure, together with the previously measured magnetic susceptibility, suggests that this material exhibits an order along its magnetic hard direction, comparable to what has been observed in other Kondo systems. An accurate determination of the CEF parameters, from techniques such as neutron spectroscopy, is required to establish the single-ion moment anisotropy that could support the hard-plane ordering scenario. Furthermore, the role of Kondo fluctuations in this peculiar phenomenon could be evidenced by chemical substitution, e.g., by replacing itinerant Ce moments with localized Nd moments [27].

[1] N. A. Spaldin and R. Ramesh, Advances in magnetoelectric multiferroics, Nat. Mater. **18**, 203 (2019).

[2] Y. F. Popov, A. M. Kadomtseva, D. V. Belov, G. P. Vorob'ev, and A. K. Zvezdin, Magnetic-field-induced toroidal moment in the magnetoelectric Cr$_2$O$_3$, J. Exp. Theor. Phys. Lett. **69**, 330 (1999).

[3] N. A. Spaldin, M. Fiebig, and M. Mostovoy, The toroidal moment in condensed-matter physics and its relation to the magnetoelectric effect, J. Phys.: Condens. Matter **20**, 434203 (2008).

[4] S. Hayami, H. Kusunose, and Y. Motome, Toroidal order in metals without local inversion symmetry, Phys. Rev. B **90**, 024432 (2014).

[5] H. Saito, K. Uenishi, N. Miura, C. Tabata, H. Hidaka, T. Yanagisawa, and H. Amitsuka, Evidence of a new current-induced magnetoelectric effect in a toroidal magnetic Ordered state of UNi$_4$B, J. Phys. Soc. Jpn. **87**, 033702 (2018).

[6] T. Ishitobi and K. Hattori, Triple-Q partial magnetic orders induced by quadrupolar interactions: Triforce order scenario for UNi$_4$B, Phys. Rev. B **107**, 104413 (2023).

[7] G. Motoyama, M. Sezaki, J. Gouchi, K. Miyoshi, S. Nishigori, T. Mutou, K. Fujiwara, and Y. Uwatoko, Magnetic properties of new antiferromagnetic heavy-fermion compounds, Ce$_3$TiBi$_5$ and CeTi$_3$Bi$_4$, Phys. B: Condens. Matter **536**, 142 (2018).

[8] G. Motoyama, M. Shinozaki, S. Nishigori, A. Yamaguchi, N. Aso, T. Mutou, M. Manago, K. Fujiwara, A. Sumiyama, and Y. Uwatoko, Transport, thermal, and magnetic properties of heavy fermion compound Ce$_3$TiBi$_5$, JPS Conf. Proc. **38**, 011084 (2023).

[9] M. P. Kwasigroch, H. Hu, F. Krüger, and A. G. Green, Magnetic hard-direction ordering in anisotropic Kondo systems, Phys. Rev. B **105**, 224418 (2022).

[10] M. Shinozaki, G. Motoyama, M. Tsubouchi, M. Sezaki, J. Gouchi, S. Nishigori, T. Mutou, A. Yamaguchi, K. Fujiwara,

K. Miyoshi, and Y. Uwatoko, Magnetoelectric effect in the antiferromagnetic ordered state of Ce_3TiBi_5 with Ce zig-Zag chains, J. Phys. Soc. Jpn. **89**, 033703 (2020).

[11] G. Bollore, M. J. Ferguson, R. W. Hushagen, and A. Mar, New ternary rare-earth transition-metal antimonides RE_3MSb_5 (RE = La, Ce, Pr, Nd, Sm; M = Ti, Zr, Hf, Nb), Chem. Mater. **7**, 2229 (1995).

[12] S. H. D. Moore, L. Deakin, M. J. Ferguson, and A. Mar, Physical properties and bonding in RE_3TiSb_5 (RE = La, Ce, Pr, Nd, Sm), Chem. Mater. **14**, 4867 (2002).

[13] M. Matin, R. Kulkarni, A. Thamizhavel, S. K. Dhar, A. Provino, and P. Manfrinetti, Probing the magnetic ground state of single crystalline Ce_3TiSb_5, J. Phys.: Condens. Matter **29**, 145601 (2017).

[14] C. Ritter, A. K. Pathak, R. Filippone, A. Provino, S. K. Dhar, and P. Manfrinetti, Magnetic ground states of Ce_3TiSb_5, Pr_3TiSb_5 and Nd_3TiSb_5 determined by neutron powder diffraction and magnetic measurements, J. Phys.: Condens. Matter **33**, 245801 (2021).

[15] T. Murakami, T. Yamamoto, F. Takeiri, K. Nakano, and H. Kageyama, Hypervalent bismuthides La_3MBi_5 (M = Ti, Zr, Hf) and related antimonides: Absence of superconductivity, Inorg. Chem. **56**, 5041 (2017).

[16] G. Motoyama, M. Shinozaki, M. Tsubouchi, M. Kuninaka, S. Nishigori, K. Miyoshi, K. Fujiwara, J. Gouchi, and Y. Uwatoko, Magnetic properties of new antiferromagnetic compound of Ce_3ZrBi_5, JPS Conf. Proc. **30**, 011180 (2020).

[17] K. Nakagawa, M. Shinozaki, G. Motoyama, S. Nishigori, K. Fujiwara, M. Manago, and K. Miyoshi, Single crystal growth of Ce_3ZrSb_5 and characterization of the physical properties, JPS Conf. Proc. **38**, 011083 (2023).

[18] S. Hayami and H. Kusunose, Magnetic toroidal moment under partial magnetic order in hexagonal zigzag-chain compound Ce_3TiBi_5, J. Phys. Soc. Jpn. **91**, 123701 (2022).

[19] J. Rodríguez-Carvajal, Recent advances in magnetic structure determination by neutron powder diffraction, Phys. B: Condens. Matter **192**, 55 (1993).

[20] K. Momma and F. Izumi, VESTA 3 for three-dimensional visualization of crystal, volumetric and morphology data, J. Appl. Crystallogr. **44**, 1272 (2011).

[21] H. T. Stokes, D. M. Hatch, and B. J. Campbell, ISODISTORT, ISOTROPY Software Suite.

[22] B. J. Campbell, H. T. Stokes, D. E. Tanner, and D. M. Hatch, ISODISPLACE : A web-based tool for exploring structural distortions, J. Appl. Cryst. **39**, 607 (2006).

[23] J. M. Perez-Mato, J. L. Ribeiro, V. Petricek, and M. I. Aroyo, Magnetic superspace groups and symmetry constraints in incommensurate magnetic phases, J. Phys.: Condens. Matter **24**, 163201 (2012).

[24] A. Biffin, R. D. Johnson, S. Choi, F. Freund, S. Manni, A. Bombardi, P. Manuel, P. Gegenwart, and R. Coldea, Unconventional magnetic order on the hyperhoneycomb Kitaev lattice in β-Li_2IrO_3: Full solution via magnetic resonant x-ray diffraction, Phys. Rev. B **90**, 205116 (2014).

[25] D. Hafner, B. K. Rai, J. Banda, K. Kliemt, C. Krellner, J. Sichelschmidt, E. Morosan, C. Geibel, and M. Brando, Kondo-lattice ferromagnets and their peculiar order along the magnetically hard axis determined by the crystalline electric field, Phys. Rev. B **99**, 201109(R) (2019).

[26] F. Krüger, C. J. Pedder, and A. G. Green, Fluctuation-driven magnetic hard-axis ordering in metallic ferromagnets, Phys. Rev. Lett. **113**, 147001 (2014).

[27] D. G. Mazzone, N. Gauthier, D. T. Maimone, R. Yadav, M. Bartkowiak, J. L. Gavilano, S. Raymond, V. Pomjakushin, N. Casati, Z. Revay, G. Lapertot, R. Sibille, and M. Kenzelmann, Evolution of magnetic order from the localized to the itinerant limit, Phys. Rev. Lett. **123**, 097201 (2019).